JOURNAL OF MAGNETIC RESONANCE **133,** 1–12 (1998)
ARTICLE NO. MN981438

EPR and DNP Properties of Certain Novel Single Electron Contrast Agents Intended for Oximetric Imaging

J. H. Ardenkjær-Larsen,*,†,[1] I. Laursen,† I. Leunbach,* G. Ehnholm,‡ L.-G. Wistrand,* J. S. Petersson,* and K. Golman*

**Nycomed Innovation AB, Ideon Malmö, S-20512 Malmö, Sweden; †Institute of Automation, The Technical University of Denmark, DK-2800 Lyngby, Denmark; and ‡Picker Nordstar Inc., Elimänkatu 24, P.O. Box 33, FIN-00511 Helsinki, Finland.*

Received September 2, 1997; revised December 11, 1997

Parameters of relevance to oximetry with Overhauser magnetic resonance imaging (OMRI) have been measured for three single electron contrast agents of the triphenylmethyl type. The single electron contrast agents are stable and water soluble. Magnetic resonance properties of the agents have been examined with electron paramagnetic resonance (EPR), nuclear magnetic resonance (NMR), and dynamic nuclear polarization (DNP) at 9.5 mT in water, isotonic saline, plasma, and blood at 23 and 37°C. The relaxivities of the agents are about 0.2–0.4 $mM^{-1}s^{-1}$ and the DNP enhancements extrapolate close to the dipolar limit. The agents have a single, narrow EPR line, which is analyzed as a Voigt function. The linewidth is measured as a function of the agent concentration and the oxygen concentration. The concentration broadenings are about 1–3 μT/mM and the Lorentzian linewidths at infinite dilution are less than 1 μT in water at room temperature. The longitudinal electron spin relaxation rate is calculated from the DNP enhancement curves. The oxygen broadening in water is about 50 μT/mM O_2 at 37°C. These agents have good properties for oximetry with OMRI.

Key Words: **EPR; DNP; contrast agents; oximetry; MRI.**

INTRODUCTION

One of the potentially interesting applications of Overhauser magnetic resonance imaging (OMRI) and electron paramagnetic resonance imaging (EPRI) is the possibility to indirectly measure the concentration of dissolved molecular oxygen (*1–5*). The oxygen partial pressure is one of the most important parameters in the metabolic processes of cells and, thus, plays an important role in many pathophysiological conditions. Many of the major types of pathology (e.g., ischemic diseases, reperfusion injury, and oxygen toxicity) are closely linked to abnormal concentrations of oxygen at particular sites in the body. In order to better understand the pathophysiological phenomena, accurate and localized measurements of oxygen concentrations are desirable. Localized or spatially resolved oxygen measurements have been given increasing attention in the last decade with the development of magnetic resonance based methods. The oxygen consumption of biological systems have been measured with spin label oximetry (*6, 7*) and oxygen mapping has been demonstrated with OMRI (*8, 9*), EPRI (*10*), and MRI (*11, 12*). Spin label oximetry represents an important advance in the technology of biological oximetry. The method is based on the observation of spectral features of exogenous paramagnetic probes. Bimolecular collisions of molecular oxygen with the contrast agent increase the relaxation rates of the electron spin of the agent. Molecular oxygen has two unpaired electrons with very short relaxation times and thus very efficiently relaxes the electron spin of the agent.

OMRI takes advantage of MRI as a mature and efficient imaging modality and the sensitivity of the electron spin relaxation rates of the single electron contrast agent to the presence of molecular oxygen. Furthermore, saturating the electron spin of the agent enhances the polarization of the water protons by a significant factor (dynamic nuclear polarization (DNP) of the Overhauser type). The DNP signal enhancement enables imaging at a low magnetic field strength. The field strength is limited by the penetration of the high EPR frequency (*13*). The EPR line of the contrast agent is saturated and, thus, requires an easily saturable resonance, otherwise leading to unacceptably high energy absorption by the patient (*13, 14*).

The purpose of this study is to give magnetic resonance properties of three new single electron contrast agents for OMRI. The agents are all based on the triphenylmethyl molecule (*15, 16*), which has been chemically modified to remove any resolved hyperfine coupling, provide water solubility, and increase the stability. The relaxivity of the agents has been measured as well as the DNP enhancements under various conditions. The EPR line shape is analyzed as a Voigt function. The change in the relaxation rates of the electron spin with agent concentration and oxygen is measured under various conditions. This study demonstrates the practicability of imaging tissue oxygen concentrations using agents such as these.

THEORY

Dynamic nuclear polarization is the transfer of electron spin polarization to the nuclear spins when the electron spin

[1] To whom correspondence should be addressed: Nycomed Innovation AB, Ideon Malmö, S-20512 Malmö, Sweden. Fax: +46 40 32 13 13. e-mail: jhal@nycomedin.ideon.se.

1090-7807/98 $25.00

transition is stimulated. In 1953, Overhauser (*17*) predicted that it should be possible to increase the amplitude of the NMR signal by stimulating the conducting electrons of a metal. The same effect applies equally well to solutions of paramagnetic agents (*18*). The rate equations for the average value of the longitudinal projection of the angular momenta, $\langle I_z\rangle$ and $\langle S_z\rangle$, for a pair of unlike spins of angular momentum I and S coupled by some time-dependent perturbing spin Hamiltonian are written

$$\frac{d\langle I_z\rangle}{dt} = -(R_{10}^I + R_1^{II})(\langle I_z\rangle - I_0) - R_1^{IS}(\langle S_z\rangle - S_0)$$

$$\frac{d\langle S_z\rangle}{dt} = -R_1^{SI}(\langle I_z\rangle - I_0) - (R_{10}^S + R_1^{SS})(\langle S_z\rangle - S_0), \qquad [1]$$

where I_0 and S_0 are the thermal equilibrium values, R_1^{II}, R_1^{IS}, R_1^{SI}, and R_1^{SS} are the relaxation rates due to the fluctuating Hamiltonian, and R_{10}^I, R_{10}^S are the sum of all other relaxation rates of the nuclear and electron spin, respectively. The steady-state solution for $\langle I_z\rangle$ is the basic DNP equation

$$\frac{\langle I_z\rangle - I_0}{I_0} = \frac{R_1^{II}}{R_1^{II} + R_{10}^I}\frac{R_1^{IS}}{R_1^{II}}\frac{S_0}{I_0}\frac{(S_0 - \langle S_z\rangle)}{S_0}. \qquad [2]$$

$R_{10}^S + R_1^{SS}$ does not explicitly enter into Eq. [2], but is related to the last factor in the equation. In the case of a single unpaired electron and a proton, the ratio of the two thermal equilibrium polarizations is equal to -658.

The coupling mechanism in most single electron contrast agent and water proton systems is entirely of dipolar origin (*19, 20*) and the transition probabilities are then (*18*)

$$R_1^{II} = r_1 c = \frac{2}{15}\left(\frac{\mu_0}{4\pi}\right)^2 \gamma_I^2\gamma_S^2 h^2 S(S+1)\{3J(\omega_I) + 7J(\omega_S)\} \qquad [3]$$

$$R_1^{IS} = \frac{2}{3}\left(\frac{\mu_0}{4\pi}\right)^2 \gamma_I^2\gamma_S^2 h^2 S(S+1)J(\omega_S), \qquad [4]$$

where γ_I and γ_S (γ_e) are the magnetogyric factors, h is Planck's constant, and μ_0 is the vacuum permeability. The relaxivity, r_1, has been introduced as the relaxation rate normalized with the concentration of the agent, c. The nuclear relaxation rate as a function of magnetic field gives the nuclear magnetic resonance dispersion (NMRD) profile. The spectral densities $J(\omega)$ are Fourier transforms of the correlation functions for the relative motion of the spins. The molecules are modeled as spin centered, hard spheres without intermolecular forces and the modulation arrives from the relative translational motion found as a solution of the simple diffusion equation (force free) (*21*)

$$J(\omega) = \frac{N_A c}{\pi D d} \times \frac{3\omega\tau + \frac{15}{\sqrt{2}}(\omega\tau)^{1/2} + 12}{(\omega\tau)^3 + 4\sqrt{2}(\omega\tau)^{5/2} + 16(\omega\tau)^2 + 27(\omega\tau)^{3/2} + 81\omega\tau + 81\sqrt{2}(\omega\tau)^{1/2} + 81}. \qquad [5]$$

The correlation time is defined as $\tau = d^2/D$, where d is the minimal distance of approach and D is the sum of the diffusion constant of the two molecules. N_A is Avogadro's number. Within the framework of this kinetic model the diffusion constants are given by the Stokes–Einstein equation,

$$D_{I,S} = \frac{k_B T}{6\pi\eta a_{I,S}}, \qquad [6]$$

where $k_B T$ is the thermal energy, η is the viscosity, and $a_{I,S}$ is the radius of the molecules.

The ratio between the relaxation rates in Eq. [2] has been split into two factors, the leakage factor f and the coupling factor k,

$$f = \frac{R_1^{II}}{R_1^{II} + R_{10}^I} = \frac{r_1 c}{r_1 c + R_{10}^I} \qquad [7]$$

$$k = \frac{R_1^{IS}}{R_1^{II}}. \qquad [8]$$

As seen from Eqs. [3] and [4], the coupling factor is one-half at low fields with a single dispersion point at $\omega_S\tau \cong 1$. The coupling factor and S_0/I_0 are often taken as one factor, $A_\infty = -329$ at low fields. The leakage factor asymptotically approaches unity as the concentration of the agent is increased.

The saturation degree of the electron spin,

$$\mathrm{SAT} = \frac{S_0 - \langle S_z\rangle}{S_0}, \qquad [9]$$

will, for a certain excitation field, depend on the electron spin relaxation rates. An inhomogeneously broadened electron spin resonance of many closely spaced hyperfine lines is very often approximated by a Voigt function, the convolution of a Lorentzian lineshape with a Gaussian intensity profile:

$$Y_v(B) = \frac{\sqrt{8}A}{\sqrt{3}\pi^{3/2}\Delta B_{pp}^L \Delta B_{pp}^G}\int_{-\infty}^{+\infty} \frac{\exp\left(-2\left(\frac{B' - B_0}{B_{pp}^G}\right)^2\right)}{1 + \frac{4}{3}\left(\frac{B - B'}{\Delta B_{pp}^L}\right)^2} dB'. \qquad [10]$$

A is the area of the function, ΔB_{pp}^G and ΔB_{pp}^L are the first

derivative peak–peak linewidths of the Gaussian and Lorentzian functions, and B_0 is the center field of the resonance. A thorough discussion and justification of this approach is given in (*22*). The convolution in Eq. [10] is in the time domain replaced by a product of the Fourier transform of the two functions (*23*)

$$Y_v(B) \leftrightarrow y_v(b) = A\,\exp(-b^2\Delta B_{pp}^{G^2}/8)\exp(-b\sqrt{3}\Delta B_{pp}^{L}/2)\exp(-iB_0 b). \quad [11]$$

To get the first derivative spectrum, which is the usual detection mode of EPR, the differentiation rule of Fourier transform pairs is used:

$$y_v(b) = -ibA\,\exp(-b^2\Delta B_{pp}^{G^2}/8) \times \exp(-b\sqrt{3}\Delta B_{pp}^{L}/2)\exp(-iB_0 b). \quad [12]$$

The Lorentzian peak–peak linewidth is related to the transverse relaxation time of the electron spin as $\Delta B_{pp}^{L} = 2(\sqrt{3}\gamma_e T_{2e})^{-1}$, which is assumed independent of the nuclear spin orientation. The longitudinal relaxation time, T_{1e}, can be calculated from the DNP enhancement curve as a function of the square of the excitation field, $B_{1e}^2 = \alpha^2 P$, with α as a resonator dependent factor, converting the incident power P to magnetic field. The saturation degree, that is, DNP enhancement curve, can be modeled as a normalized sum of the off-resonance saturation of the individual hyperfine lines of the inhomogeneously broadened resonance. In the Voigt case expressed as the integral

$$\frac{\langle S_z(B)\rangle}{S_0} = \sqrt{\frac{2}{\pi}}\frac{1}{\Delta B_{pp}^{G}} \times \int_{-\infty}^{+\infty} \frac{\exp\left(-2\left(\frac{B'-B_0}{\Delta B_{pp}^{G}}\right)^2\right)\left(1+\frac{4}{3}\left(\frac{B-B'}{\Delta B_{pp}^{L}}\right)^2\right)}{1+\frac{4}{3}\left(\frac{B-B'}{\Delta B_{pp}^{L}}\right)^2+\alpha^2 P\,\frac{\sqrt{3}\gamma_e T_{1e}}{2\Delta B_{pp}^{L}}}\,dB', \quad [13]$$

which need only be evaluated on-resonance, $B = B_0$, when combined with the analysis of the EPR spectrum. However, DNP enhancement curves as a function of B and P enable full assessment of ΔB_{pp}^{G}, ΔB_{pp}^{L}, and $2/\sqrt{3}\gamma_e T_{1e}$ (the longitudinal relaxation rate; i.e., 6.56 μT μs divided by T_{1e} in microseconds). α needs to be calibrated by some other means. For on-resonance irradiation it is convenient to specify the irradiation field, $(B_{1e})_{1/2} = \alpha\sqrt{P_{1/2}}$, at half saturation of the EPR line. At this circular amplitude of the irradiation field, half the maximum DNP enhancement is obtained for the particular concentration of the agent.

An electron spin is generally coupled to nuclear spins in the molecule by hyperfine interactions giving well-resolved resonance lines. The effect of hyperfine structure is to reduce the DNP enhancement by a factor, given as the fraction of spins contributing to the nonsaturated resonance lines relative to the total number of spins. More stringently, it will be the integration of Eq. [9] across the entire spectrum taking into account cross-saturation and the effect of the excitation field on each resonance line.

In spin label oximetry the following equation is generally applied to the exchange broadening of the agent (*6*, *7*),

$$\Delta B_{pp} = \frac{8\pi}{\sqrt{3}\,\gamma_e} pr_0\{D_{agent} + D_{O_2}\}N_A c_{O_2}, \quad [14]$$

stating that the peak–peak line broadening is proportional to the oxygen concentration, c_{O_2}, the sum of the diffusion constants, $D_{agent} + D_{O_2}$, an interaction radius, r_0, and the probability that an exchange process will occur during collision, p. The probability of spin exchange with oxygen is believed to be close to one for most spin labels at physiological conditions (*6*, *7*). In that case the efficiency of a T_{2e} and T_{1e} process is predicted theoretically to be equal (*24*). However, Subczynski and Hyde (*25*) predict a ratio of 2/3 of the efficiency of a T_{1e} and T_{2e} process. The oxygen–agent interaction is dominated by Heisenberg spin exchange and the dipole–dipole interaction can in most cases be neglected (*25*).

The oxygen sensitivity of the DNP enhancement factor can be considered by looking at the change in signal, S, for a small change in oxygen concentration,

$$\mathrm{SAT} \cong \frac{(\gamma_e B_{1e})^2}{(\gamma_e (B_{1e})_{1/2})^2 + (\gamma_e B_{1e})^2} = \frac{(\gamma_e B_{1e})^2}{(A + Bc_{O_2})^2 + (\gamma_e B_{1e})^2} \quad [15]$$

$$\frac{\partial S}{\partial c_{O_2}} = \frac{\partial \mathrm{SAT}}{\partial c_{O_2}} = \frac{-(\gamma_e B_{1e})^2 B 2(A + Bc_{O_2})}{((A + Bc_{O_2})^2 + (\gamma_e B_{1e})^2)^2}, \quad [16]$$

where $(B_{1e})_{1/2}$ has been approximated by the expression $A + Bc_{O_2}$. A is an effective relaxation rate in the absence of oxygen and Bc_{O_2} is the oxygen contribution. The maximal sensitivity is found for $\gamma_e B_{1e} = \gamma_e (B_{1e})_{1/2} = A + Bc_{O_2}$:

$$\frac{\partial S}{\partial c_{O_2}} = \frac{-B}{2(A + Bc_{O_2})}. \quad [17]$$

Thus, if the oxygen broadening is the dominant contribution to the relaxation rates ($Bc_{O_2} > A$), an optimal oxygen sensitivity is obtained.

The relaxation rates of the electron spin are also dependent on the concentration of the agent. Intermolecular Heisenberg

spin exchange and dipole–dipole interaction will increase the relaxation rates of the electron spin, and lower the saturation degree for a certain power level. The dipole–dipole interaction for like spins can be calculated according to (*18*)

$$\frac{1}{T_{1e}} = \frac{2}{5}\left(\frac{\mu_0}{4\pi}\right)^2 \gamma_S^4 h^2 S(S+1)\{J(\omega_S) + 4J(2\omega_S)\} \quad [18]$$

$$\frac{1}{T_{2e}} = \frac{1}{5}\left(\frac{\mu_0}{4\pi}\right)^2 \gamma_S^4 h^2 S(S+1) \times \{3J(0) + 5J(\omega_S) + 2J(2\omega_S)\}, \quad [19]$$

where all symbols have been defined previously. The contribution from Heisenberg spin exchange is given by an expression analogous to Eq. [14] (*42*),

$$\Delta B_{pp} = \frac{16\pi}{\sqrt{3}\gamma_e} p r_0 D_{agent} N_A c. \quad [20]$$

For ionic molecules the spectral densities of Eqs. [18] and [19] are found by calculating the correlation functions from the Smoluchowski diffusion equation with a molecular potential $V(r)$. In the simplified continuum model (*26*) the Coulomb potential is

$$V(r) = \frac{q_1 q_2}{4\pi\epsilon r} \frac{\exp(-\kappa(r-d))}{1+\kappa d}, \; r > d, \quad [21]$$

where κ^{-1} is the Debye length,

$$\kappa = \sqrt{\frac{2IN_A e^2}{\epsilon k_B T}}, \quad I = \frac{1}{2}\sum_i c_i z_i^2. \quad [22]$$

The summation is running over all ionic species of concentration c_i and charge $q_i = z_i e$. ϵ is the dielectric constant of the medium and d is the minimal distance of approach. The potential $V(r)$ expresses the ionic screening of the attractive or repulsive force between the pair by counterion clustering. For a pair of negatively charged molecules the repulsive force at low ionic strengths decreases the amplitude of Eqs. [18]–[20] up to a certain concentration, where the association with counterions or formation of a charge-screening ionic atmosphere reduces the effective charge of the radical and the broadening increases. According to the theory of Debye the diffusion constant of spherical, charged ions in very dilute solutions is given as

$$D_{ion} = \frac{V(d)}{k_B T} \frac{1}{\exp(V(d)/k_B T) - 1} D; \quad [23]$$

where D is the diffusion constant of the neutral molecule. The Heisenberg spin exchange of ionic agents, Eq. [20], must be modified accordingly. The efficiency of the exchange process, p, may also be changed by the electrostatic forces (*42*).

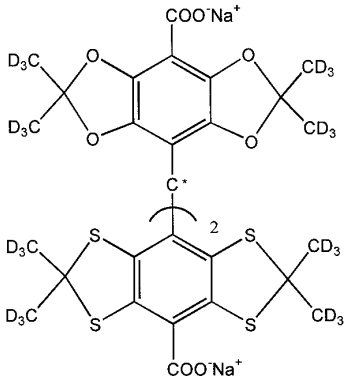

Perdeuterated trityl. MW=1080.

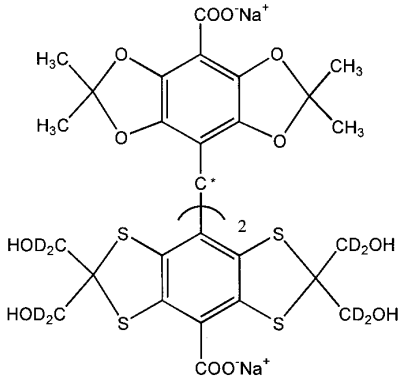

Deuterated hydroxy trityl. MW=1145.

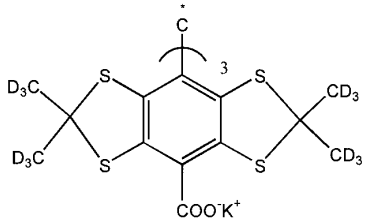

Symmetric trityl. MW=1151.

FIG. 1. Structure, abbreviations, and formula weight for the three examined triphenylmethyls.

MATERIALS AND METHODS

Single Electron Contrast Agents

Three different triphenylmethyl agents have been examined. Their chemical formulae and names are given in Fig. 1 (*15, 16*). The three agents are obtained as dry substances. They are sodium or potassium salts of tricarboxylic acids and the pH has been adjusted to 7. The purity of the agents is >97% as determined by HPLC. Two of the trityls bind

strongly to proteins and the degree of protein binding has been determined as follows: Solutions of 5% weight human serum albumin (Sigma Chemical Co., essentially free of fatty acids) corresponding to a concentration of 0.8 mM were prepared in 0.9% NaCl distilled water and a 0.05 M sodium phosphate buffer, pH 7. The agents were dissolved in the albumin solution at concentration levels 1, 3, and 10 mM at room temperature. After ultrafiltration of the solutions, the amounts of agent in the protein filtrates were determined by HPLC. The perdeuterated and symmetric trityl showed fractional bindings to albumin of 50% and 80%, respectively, and the deuterated hydroxy trityl only showed about 5% albumin binding.

In deoxygenated water the stability varied from a half-life of 6 days for the deuterated hydroxy trityl to more than a year for the symmetric trityl. The three agents are all stable to oxygen. In human blood at 37°C the stability varied from a half-life of a few hours for the deuterated hydroxy trityl to much more than 24 hours for the symmetric trityl. Thus, the three trityls can be considered stable during the course of experiments.

Sample Preparation

Samples were prepared in distilled water, isotonic saline (0.15 M sodium chloride in distilled water), human plasma, and human whole blood. Venous blood was collected in preheparinized vacuum tubes for immediate use. Plasma was obtained from the venous blood by centrifugation at 720*g* for 5 min. The agent was weighted as dry substance and dissolved in the medium of interest. The sample was sealed with a rubber septum. Decreasing concentrations were prepared by diluting the sample with the solvent in question.

The various oxygen partial pressures of the solvents were obtained in a custom-built shaking tonometer. The sample of 1–2 ml volume was shaken with a vapor-saturated gas mixture flowing slowly above the sample for at least 5–10 min, dependent on the solvent. The sample and gas were kept in a thermostat. The gases were high-purity, chemically analyzed mixtures of 5% CO_2, some fraction O_2, and the rest N_2 (AGA, Sweden). This principle of oxygenation is generally accepted to be accurate and reproducible (*27*) for blood and plasma oxygenation. The oxygen concentration is calculated as

$$c_{O_2} = \frac{\alpha\, F(P_B - P_w)}{760 \times 22.463} \times 10^3\,(\mathrm{mM}), \qquad [24]$$

where α is the Bunsen solubility factor at STPD conditions, F is the fraction of oxygen in the gas mixture, P_B is the pressure of the gas, and P_w is the vapor pressure, both in torr.

Apparatus and Methods

The NMRD profiles were obtained on a field-cycling relaxometer (*28*). All the EPR and DNP data was obtained on a custom-built 9.5-mT EPR and DNP spectrometer. The sample is thermostatically controlled in the resonator by a perfluorinated liquid, Fluorinert™ FC-104 (3M, Sweden), flowing inside a double-walled glass tube. The temperature is controlled to within ±0.1°C with an absolute accuracy of ±0.5°C (sum of measurement error and effect of temperature gradient). A loop-gap resonator is mounted on the thermostat with a shield of folded copper foil. The copper foil is a short circuit at the EPR frequency of 267 MHz and open at the NMR frequency of 404 kHz. A solenoid tuned for the proton frequency is wound on the shield of the loop-gap resonator. The EPR data is recorded as continuous wave, field swept, and field modulated spectra. The detection is homodyne with a double balanced mixer. The NMR spectrometer is pulsed. An arbitrary waveform generator creates the pulse sequence and a circuitry isolates the preamplifier during the pulses.

The EPR excitation field is calibrated from the progressive saturation spectra of Fremy's salt. The peak–peak linewidth and lineheight of the central line is recorded as a function of incident power. The linewidth of Fremy's salt does not differ significantly from 267 MHz to X-band. Therefore, a T_{2e} of 0.26 μs and a T_{1e} of 0.34 μs at room temperature and in equilibrium with air has been used (*29*). The value obtained is a circular amplitude of 2.60 $\mu\mathrm{T}/\sqrt{\mathrm{mW}}$. This is in accordance with the value calculated from the formulae (critically coupled resonator) (*30*)

$$Q_L = \frac{\omega_0 W_s}{P_{loss}} = \frac{\omega_0 W_s}{P_{in}} \qquad [25]$$

$$W_s = \frac{1}{2\mu_0} B_{1e}^2 \pi r_0^2 (z + \Delta z)(1 + p),$$

$$\Delta z \approx 0.18R \text{ and } p = \frac{r_0^2}{R^2 - r_0^2}, \qquad [26]$$

where P_{in} is the incident power, W_s the stored energy, r_0 the loop-gap radius, R the radius of the shield, and z the length of the resonator. Inserting the loop-gap dimensions $r_0 = 1$ cm, $R = 2$ cm, and $z = 4.5$ cm, the resonance frequency of 267 MHz and a measured Q_L of 380 with the sample gives a linearly polarized B_1 of 5.28 $\mu\mathrm{T}/\sqrt{\mathrm{mW}}$. A value of 2.60 $\mu\mathrm{T}/\sqrt{\mathrm{mW}}$ has been used in the DNP experiments with the appropriate Q corrections (the Q is measured as a function of the sample loading).

EPR data acquisition and analysis was performed on a standard PC interfaced with a GPIB to the spectrometer instruments. The EPR spectrum was iteratively fitted to the theoretical expression Eq. [12] in the time domain. A Lorentzian lineshape can be imposed on the data by choosing ΔB_{pp}^G equal to zero as starting value. The time domain approach increases the speed of the fitting procedure by more than an order of magnitude. The fitting procedure is a

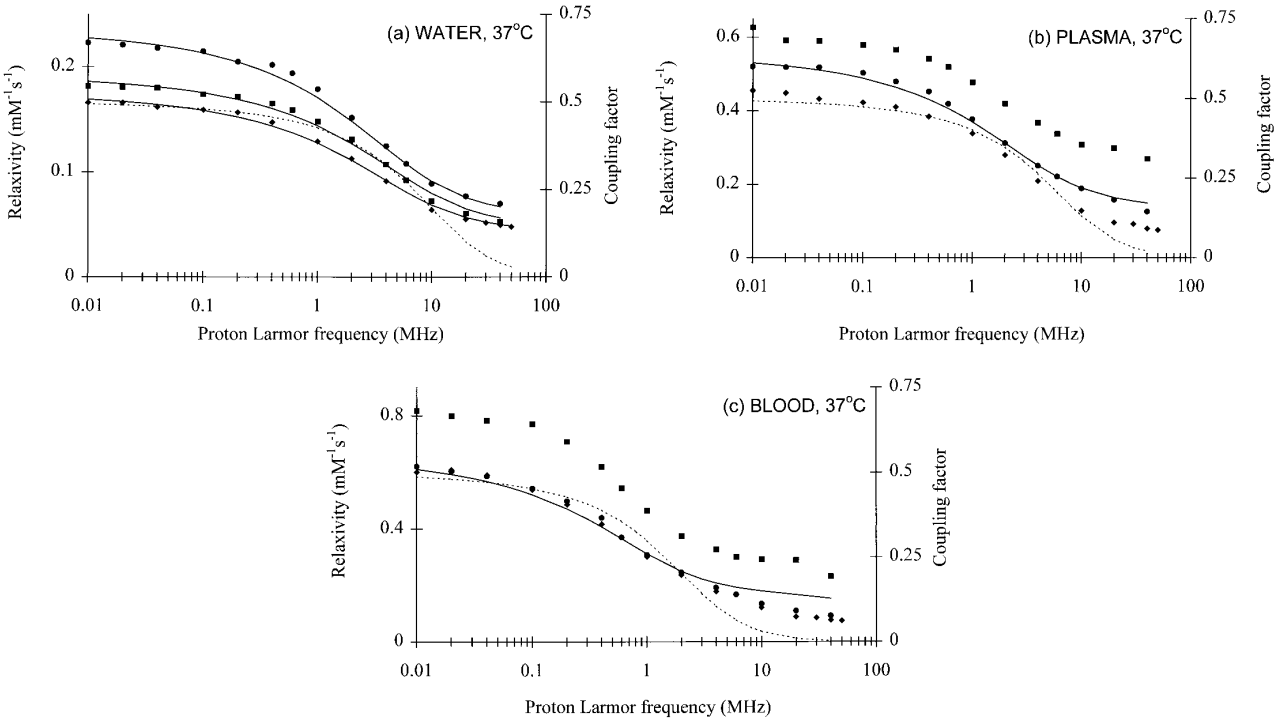

FIG. 2. NMRD profiles of (●) deuterated hydroxy trityl, (■) symmetric trityl, and (◆) perdeuterated trityl in (a) water, (b) plasma and (c) blood at 37°C. (—) Least-squares fit of Eqs. [3] and [5] to (a) the three NMRD profiles and (b) and (c) the deuterated hydroxy trityl NMRD profile. The minimal distances of approach and correlation times can be found in Table 1. (----) (a)–(c) The coupling factor, Eq. [8], with the correlation time obtained from the fit to NMRD profile for the deuterated hydroxy trityl.

standard Levenberg–Marquardt algorithm (*31*) and error estimates are obtained from the covariance matrix. The same fitting algorithm was used to fit saturation recovery data to an exponential function to obtain the proton T_1 and to fit the DNP enhancement data to Eq. [13].

EXPERIMENTAL RESULTS

The solvent proton relaxation rate for a certain concentration of the agent has been measured for the three trityls as a function of magnetic field strength in water, human plasma, and human whole blood at 37°C. The relaxivities of the agents

TABLE 1
Parameters Obtained from the Least-Squares Fit of Eqs. [3] and [5] to the NMRD Profiles

	Minimum distance of approach d (nm)	Relative diffusion const. $D \times 10^9$ (m^2/s)	Correlation time τ_D (ps)	Ratio of diffusion constants D_{37}/D_{23}
Perdeuterated trityl				
Water at 23°C	0.58 ± 0.01	1.9 ± 0.2	178 ± 14	1.4
at 37°C	0.60 ± 0.01	2.7 ± 0.2	132 ± 9	
Deuterated hydroxy trityl				
Water at 23°C	0.53 ± 0.01	1.7 ± 0.2	166 ± 12	1.3
at 37°C	0.54 ± 0.01	2.1 ± 0.2	137 ± 9	
Plasma at 23°C	0.49 ± 0.02	0.9 ± 0.3	258 ± 25	1.2
at 37°C	0.47 ± 0.02	1.1 ± 0.3	207 ± 20	
Blood at 23°C	0.61	0.6	637	1.0
at 37°C	0.68	0.6	733	
Symmetric trityl				
Water at 23°C	0.55 ± 0.02	1.9 ± 0.02	156 ± 13	1.4
at 37°C	0.54 ± 0.02	2.7 ± 0.02	110 ± 9	

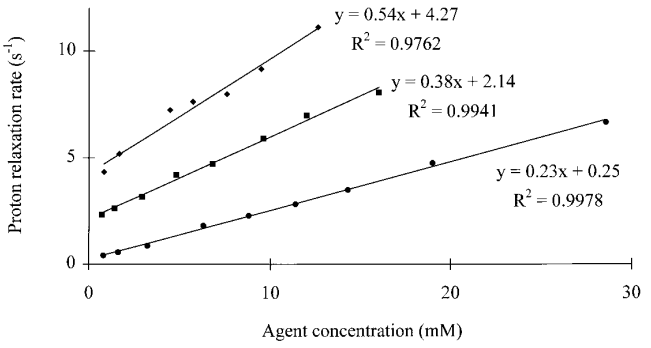

FIG. 3. Proton relaxation rate of (●) water, (■) plasma, and (◆) blood as a function of the concentration of the deuterated hydroxy trityl at 37°C.

are shown in Figs. 2a–2c. The parameters obtained from the fits to the NMRD profiles are given in Table 1.

The linearity of the relaxivity with concentration, Eq. [3], has been confirmed and is plotted in Fig. 3 for the deuterated hydroxy trityl.

The water proton DNP enhancement, Fig. 4, for the deuterated hydroxy trityl in water, plasma, and blood at 37°C and for full saturation of the EPR line was measured as a function of the agent concentration. The DNP enhancement for the perdeuterated trityl in water and plasma at 37°C is also shown. The relaxivities and enhancements at infinite concentration of the agents obtained from the fits of Eqs. [2] and [7] with SAT = 1 to the measured DNP enhancement curves are given in Table 2.

The EPR spectrum of the deuterated hydroxy trityl is shown in Fig. 5, and the Voigt function has been fitted to the central resonance, Fig. 6. The Gaussian linewidth, ΔB_{pp}^{G}, of the perdeuterated trityl is 2.05 μT, of the deuterated hydroxy trityl 5.40 μT, and of the symmetric trityl 2.10 μT. The peak–peak linewidth and the Lorentzian linewidth are obtained from the Voigt lineshape analysis of the EPR spectrum in water, Fig. 7.

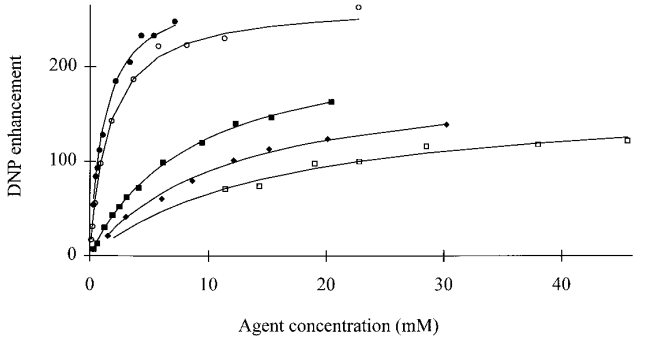

FIG. 4. DNP enhancements, $(\langle I_z \rangle - I_0)/I_0$, at full saturation of the EPR line as a function of concentration for the deuterated hydroxy trityl in (●) water, (■) plasma, and (◆) blood at 37°C and the perdeuterated trityl in (○) water and (□) plasma at 37°C. (—) Least-squares fits of Eqs. [2] and [7] with SAT = 1; relaxivities and enhancement at infinite concentration can be found in Table 2.

TABLE 2

Relaxivity and Enhancement at Infinite Concentration and Power Obtained from the DNP Enhancement Data for the Three Trityls

	r_1 ($mM^{-1}s^{-1}$)	A_∞
Perdeuterated trityl		
In water at 23°C	0.19	−267
at 37°C	0.14	
Deuterated hydroxy trityl		
In water at 23°C	0.26	−278
at 37°C	0.20	
Plasma at 37°C	0.32	−231
Blood at 37°C	0.44	−192
Symmetric trityl		
In water at 23°C	0.21	−266
at 37°C	0.15	

The Lorentzian linewidth in isotonic saline is also shown. The Lorentzian linewidth is a linear function of concentration in isotonic saline, and the slopes and intercepts of the linear regression fits for the three trityls at 23 and 37°C in the deoxygenated solvent are given in Tables 3 and 4. The same analysis is performed for the deuterated hydroxy trityl in plasma and blood at 37°C, Table 4.

The longitudinal relaxation rate, Fig. 8, is obtained from the analysis of the measured DNP enhancement curve as a function of the saturating magnetic field. Equation [13] with $B = B_0$ is fitted to the DNP enhancement curve (ΔB_{pp}^{G} and ΔB_{pp}^{L} are obtained from the analysis of the EPR spectrum). Tables 3 and 4 give the linear regression analysis of the measurements in isotonic saline. The deuterated hydroxy trityl has been measured in plasma and blood at 37°C as well (Table 4). The EPR excitation field at half the maximum DNP enhancement, $(B_{1e})_{1/2}$, has been measured in all four solvents for the deuterated hydroxy trityl (Fig. 9).

For the deuterated hydroxy trityl, the Lorentzian linewidth and the longitudinal relaxation rate have been measured as a function of oxygen concentration, Fig. 10. Table 5 gives the slopes of the linear regression analysis to the data, and the dependence of the EPR excitation field at half the maximum DNP enhancement on the oxygen concentration.

FIG. 5. EPR spectrum of the deuterated hydroxy trityl in water at room temperature. ^{13}C satellites are shown enlarged.

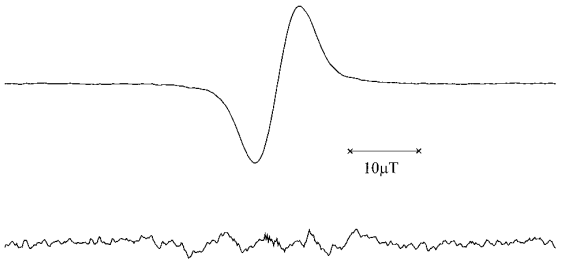

FIG. 6. EPR spectrum of the deuterated hydroxy trityl with the Voigt fit and residue ×10. The Gaussian and Lorentzian line widths are 5.42 and 1.64 μT, respectively, and the peak–peak line width is 6.30 μT. The closest ^{13}C satellites appear in the residue undistorted.

TABLE 3
Relaxation Rates at Infinite Dilution in Deoxygenated Isotonic Saline

	$2(\sqrt{3}\gamma_e T_{1e})^{-1}$ (μT)	$2(\sqrt{3}\gamma_e T_{2e})^{-1}$ (μT)
Isotonic saline at 23°C		
Perdeuterated trityl	0.8 ± 0.1	0.9 ± 0.1
Deuterated hydroxy trityl	0.7 ± 0.2	1.0 ± 0.2
Symmetric trityl	0.8 ± 0.1	0.8 ± 0.1
Isotonic saline at 37°C		
Perdeuterated trityl	0.5 ± 0.1	0.8 ± 0.1
Deuterated hydroxy trityl	0.6 ± 0.2	0.8 ± 0.2
Symmetric trityl	0.7 ± 0.1	0.7 ± 0.1

Note. Standard deviations are indicated for each of the values.

DISCUSSION

The diffusion constants obtained from the NMRD profiles in water varies according to the Stokes–Einstein equation. The viscosity of water is 0.93 cp at 23°C and 0.69 cp at 37°C (*32*). Thus, the ratio of η/T at the two temperatures is 1.4. The agreement between the measured data and the model function is considered good. The minimal distances of approach are found consistent with the average radius of the molecules based on molecular mechanics, and the relative diffusion constants are also found reasonable. The diffusion constants calculated from the Stokes–Einstein equation at 23 and 37°C in water for a molecular radius of 0.4 nm (the average of the minimal distances of approach minus a water radius) are 0.6×10^{-9} m^2/s and 0.8×10^{-9} m^2/s, respectively. This is about one-third of the relative diffusion constants of Table 1. The effect of water proton eccentricity has been found to be very small, as can be seen from a series expansion of the spectral densities in the eccentricity parameter (the distance from the spin center to the molecule center relative to the molecular radius) (*33*). For the molecular dimensions of the three agents, the higher order expansion coefficients are negligible, particularly at low frequencies. The same qualitative deviation in the fits to the NMRD profiles in water just above the dispersion point is generally seen for other agents (*34*) and is probably due to the neglect of pair correlation effects. First of all, the usual pair correlation effects are expressed in the Verlet and Weiss (*35*) pair correlation function or as a solution of the Percus–Yevick equation (*36, 37*). The NMRD profiles in plasma and blood are not as easily explained. The agents are interacting with plasma components and red blood cells. The protein binding of two of the triphenylmethyls causes a much more complicated dispersion profile. The fit to the deuterated hydroxy trityl is still good, but with an error increasing from plasma to blood. The temperature dependence of the diffusion constant no longer follows the Stokes–Einstein equation. The uncertainty of the parameters is greater and the model function does not explain the profiles.

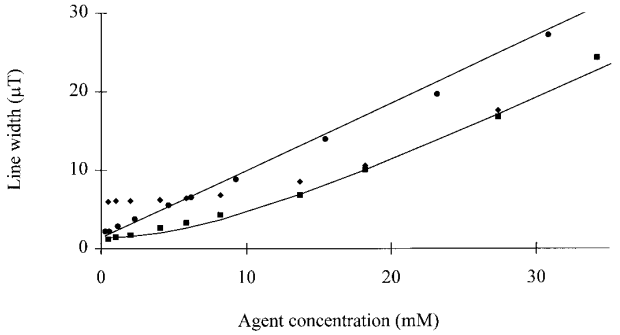

FIG. 7. (◆) The peak–peak linewidth and (■) the Lorentzian linewidth, $2(\sqrt{3}\gamma_e T_{2e})^{-2}$, from Voigt lineshape analysis in water, and (●) the Lorentzian linewidth in isotonic saline for the deuterated hydroxy trityl at 37°C. (—) Linear regression fit in isotonic saline and fit to Eq. [23] in water.

From Figs. 2a–2c it can be seen that the relaxivity cannot be increased by a further slowing of the relative translational motion (e.g., by trying to introduce pair correlation effects). The relaxivity will only increase weakly at 400 kHz and the coupling factor is approaching the dispersion point.

The increased leakage of proton magnetization through other relaxation paths is observed in Fig. 4 for the deuterated hydroxy trityl. The water proton relaxation rate of plasma and blood at low field are much larger than the relaxation rate of neat water, Fig. 3. The relaxivities obtained from the fits are in good agreement with the values obtained from the NMRD profile. The DNP enhancement is to the first order of magnitude not affected by temperature at low fields, since the relaxivity of the agent and relaxation time of the solvent have inverse dependencies on temperature. The enhancement factor, A_∞, is reduced significantly from -329, the maximum enhancement in the dipolar limit. The loss of enhancement due to the ^{13}C (natural abundance of 0.0111) satellites is estimated as 10 well-resolved hyperfine lines, based on Figs. 1 and 7, leading to a reduction factor of 0.89 (0.9889^{10}). The coupling factors at 400 kHz and 37°C are 0.46 in water, 0.44 in plasma, and 0.39 in blood, Figs. 2a–2c. Taking these factors into account the DNP data confirms the assumption that the coupling between the water protons and the electron spin is exclusively dipolar. The reduction of the enhancement at infinite

TABLE 4
Increase in Relaxation Rates with Agent Concentration

	$2(\sqrt{3}\gamma_e T_{1e})^{-1}$ (μT/mM)	$2(\sqrt{3}\gamma_e T_{2e})^{-1}$ (μT/mM)
Isotonic saline at 23°C		
Perdeuterated trityl	1.06 ± 0.08	2.43 ± 0.08
Deuterated hydroxy trityl	0.26 ± 0.05	1.11 ± 0.05
Symmetric trityl	1.32 ± 0.05	3.54 ± 0.06
Isotonic saline at 37°C		
Perdeuterated trityl	1.29 ± 0.03	2.81 ± 0.12
Deuterated hydroxy trityl	0.28 ± 0.02	0.80 ± 0.02
Symmetric trityl	1.77 ± 0.08	3.31 ± 0.03
Deuterated hydroxy trityl at 37°C		
in plasma	0.27 ± 0.05	0.98 ± 0.05
in blood	0.36 ± 0.05	2.15 ± 0.05

Note. Standard deviations are indicated for each of the values.

concentration in plasma and blood is somewhat greater than expected from these factors. In these two media the variation in the parameters is about ±10% from series to series, assumed to be the effect of natural variations in the blood-sample donations. However, the further reduction appears to be significant. The reason may be the three spin effect (*38*). A biological system is not a homogeneous proton system, but consists of water protons, protein protons, and lipid protons. The DNP enhancement will in principle depend on the transfer of magnetization between these proton systems. For the perdeuterated trityl in water the enhancement extrapolates close to the dipolar limit. In plasma a dramatic reduction is observed: The infinite-concentration DNP enhancement extrapolates to about 100. The reason for this quench of the DNP enhancement appears to be the protein binding of ca. 50%, accounting for the observed reduction. Thus, from these two agent examples protein binding is considered undesirable. Therefore, only the deuterated hydroxy trityl was characterized in plasma and blood with EPR and DNP.

The triphenylmethyl molecule is well known and has previously been studied by EPR and ENDOR (*39*, *40*). The uniqueness of the single electron contrast agents examined is their

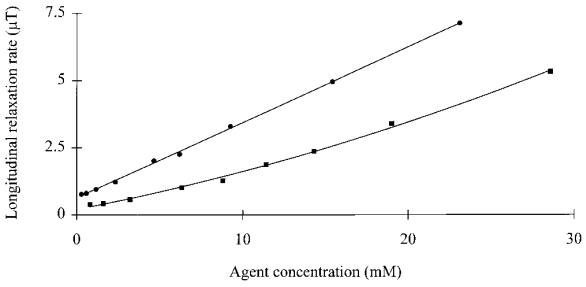

FIG. 8. $2(\sqrt{3}\gamma_e T_{1e})^{-1}$, from the analysis of the DNP enhancement curve in (■) water and (●) isotonic saline for the deuterated hydroxy trityl at 37°C. (—) Linear regression fit in isotonic saline and fit to Eq. [23] in water.

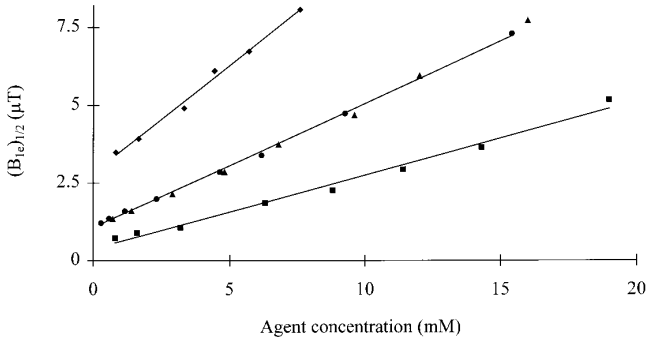

FIG. 9. The EPR excitation field at half the maximum DNP enhancement, $(B_{1e})_{1/2}$, for the deuterated hydroxy trityl in (■) water, (●) isotonic saline, (▲) plasma, and (◆) blood at 37°C. (—) Linear regression fits.

stability, their water solubility, and the removal of resolved hyperfine structure, Fig. 5. The triphenylmethyls described in this investigation only display resolved hyperfine couplings to the ^{13}C nuclei in the molecule. However, the single resonance is inhomogeneously broadened and it is perfectly fitted by the Voigt function, Fig. 6. The residue does not display any systematic error apart from the nearest ^{13}C satellites appearing undistorted. The ratio between the Gaussian and Lorentzian peak–peak linewidths is 3.3 and the fit appears to be perfect as expected on the basis of the large number of unresolved deuterium and/or proton couplings. The Gaussian linewidth was observed to be independent of or to decrease slightly with increasing concentration of the agent, due to an averaging of the unresolved hyperfine couplings. From Table 3 it is seen that the intrinsic (Lorentzian) linewidth is very narrow at infinite dilution in water. It is noticed that the linewidth decreases with increasing temperature, excluding spin-rotational relaxation as the dominant contribution. Probably, the linewidth is caused by small anisotropies in the *A* tensor couplings to the protons/deuterons. Since the linewidth does not increase at X-band, *g* tensor anisotropy is not believed to dominate. Finally, the nuclear–nuclear quadrupole interaction can cause electron spin relaxation (*41*), and the dipolar interaction with the solvent

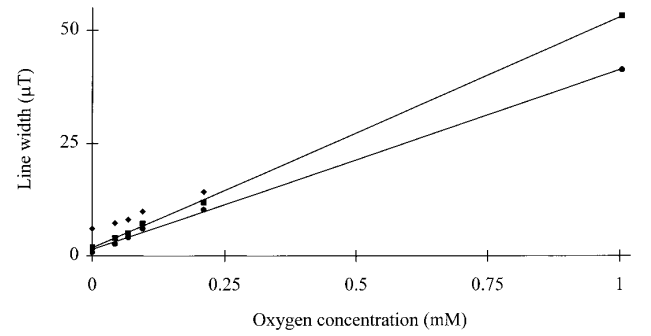

FIG. 10. The oxygen effect on (◆) the peak–peak linewidth, (■) the Lorentzian linewidth, $2(\sqrt{3}\gamma_e T_{2e})^{-1}$, and (●) $2(\sqrt{3}\gamma_e T_{1e})^{-1}$, for the deuterated hydroxy trityl in water at 37°C. (—) Linear regression fits.

TABLE 5

Increase in Relaxation Rates and the EPR Excitation Field at Half the Maximum DNP Enhancement, $(B_{1e})_{1/2}$, with Oxygen Concentration for the Deuterated Hydroxy Trityl

	$(B_{1e})_{1/2}$ (μT/mM O_2)	$2(\sqrt{3}\gamma_e T_{1e})^{-1}$ (μT/mM O_2)	$2(\sqrt{3}\gamma_e T_{2e})^{-1}$ (μT/mM O_2)
Water at 37°C	35.9	39.8	51.1
at 23°C	28.2	30.1	36.9
Blood at 37°C	31.9	33.0	42.8
at 23°C	24.9	25.0	32.9

protons is found by multiplying the relaxivity with the proton density in millimolar (110,000 mM for water), giving about 0.2 μT (R_1^{SS} is obtained from Eq. [3] by permutation of indices). The transverse and longitudinal relaxation rates are very close at infinite dilution.

The concentration-dependent broadening is nonlinear in water. The electrostatic repulsion from the three negative charges of the carboxylic acids reduces the interaction between the molecules. Above about 10 mM, the broadening increases and finally becomes a linear function of concentration. In isotonic saline the electrostatic repulsion is completely screened and the linewidth becomes a linear function of concentration, Figs. 7 and 8. The change in relaxation rates with concentration is seen to be much smaller than usually observed for nitroxide agents (*42*). The self-broadening of the deuterated hydroxy trityl is about one-tenth of the value observed for a nitroxide agent. The small slope of the broadening of the deuterated hydroxy trityl and the dependence on temperature and viscosity lead to the assumption that the mechanism is predominantly dipolar. With the longitudinal relaxation rates of the deuterated hydroxy trityl in water at 23 and 37°C, Table 4, a minimal distance of approach of 1.1 nm is calculated from Eq. [18] when the diffusion constants from the Stokes–Einstein equation, 0.6×10^{-9} m^2/s ($\tau = 1.0$ ns) and 0.8×10^{-9} m^2/s ($\tau = 0.76$ ns), are used. Equation [19] gives 75% and 90%, respectively, of the transverse relaxation rate with the same parameter values. The larger minimal distance of approach (1.1 nm as opposed to the molecular radius of 0.4 nm from the NMRD profile) can be explained by the counterion clustering in the agent–agent encounter. A curve of the functionality of Eq. [23] has been fitted to the water data points. The initial slope ($\kappa = 0$) relative to the slope at high concentrations ($\kappa \to \infty$) is equal to $q_1 q_2/\epsilon d k_B T \times (\exp(q_1 q_2/\epsilon d k_B T) - 1)^{-1}$ (*42*). The value of this expression is 0.02 in water for $d = 1.1$ nm and $q_1 q_2 = 9$. The measured value is 0.06. The uncertainty of the initial slope is, however, relatively large. In plasma and blood the relaxation rates have increased as expected from the increase of viscosity of the media. For the two other tritylys the broadening is larger and the temperature variation is not consistent with the assumption of dipolar interaction. Thus, Heisenberg spin exchange is believed to contribute significantly for these two tritylys.

The EPR excitation field at half saturation of the EPR line, Fig. 9, is a linear function of concentration in all four media. The nonlinearity of the relaxation rates in water is obscured because of the inhomogeneous broadening. At low concentrations more power is needed to saturate because of the inhomogeneous line width, which is decreasing with the increasing concentration.

The oxygen line broadening is 51.1 μT/mM O_2 in water at 37°C. The oxygen diffusion constant is 3.1×10^{-9} m^2/s at 37°C (*43*) and 2.1×10^{-9} m^2/s at 25°C (*44*), much greater than the trityl diffusion constant. From Eq. [14] a product of the exchange probability and interaction radius of 0.33 nm is obtained. This radius is smaller than expected when compared with the minimal distance of approach from the NMRD profile. A steric factor may be introduced into Eq. [14], taking into account collision that does not cause spin exchange or spin dephasing (*42*). The ratio of the oxygen broadening in water at 23 and 37°C is 0.72, close to the ratio of the oxygen diffusion constants. Thus, the relaxation process appears to be diffusion limited as expected. The ratio between the transverse and longitudinal relaxation rates is 0.69, very close to the value predicted in (*25*). The exact theory of the spin exchange efficiency with oxygen appears not to be well understood. Apparently some collisions are spin dephasing and do not result in an exchange of spin states. Table 5 also gives the EPR excitation field at half the maximum DNP enhancement dependence on oxygen. It is interesting to notice that in blood at 37°C the oxygen effect is 31.9 μT/mM O_2, 46 times more than the agent concentration effect of 0.66 μT/mM ($(\gamma_e \sqrt{T_{1e} T_{2e}})^{-1}$ obtained from the values in Table 4). Thus, in the physiological range the oxygen contribution to $(B_{1e})_{1/2}$ is about 3.2 μT, about five times the agent concentration contribution and a doubling of the value from the deoxygenated state.

All the relaxation data is dependent on an accurate calibration of the EPR excitation field. Considering the very good agreement between the field calibration obtained with Fremy's salt and the calculated value, the systematic error in the T_{1e} data is believed to be negligible. Correcting for the variations in the Q value of the resonator with temperature and sample loading significantly improves the estimation of the longitudinal relaxation rate.

CONCLUSION

The single electron contrast agents examined have unique properties that are due to their water solubility, their stability, and a single and narrow EPR resonance. This enables high DNP enhancements at moderate power levels and concentrations in the millimolar range. The DNP enhancements of the agents extrapolate close to the dipolar limit. The relaxivity is well modeled and in full agreement with the expected value for a $S = 1/2$ system. In biological fluids at low field the proton relaxation rate is so short that significant leakage of magneti-

zation cannot be prevented at reasonable concentrations, and a less than maximal enhancement must be accepted.

We have investigated the EPR saturation properties of three novel single electron contrast agents. The relaxation times of these agents under physiological conditions may be sufficiently long to impose no limitations on OMRI from the energy absorption of the patient.

The sensitivity of these agents to oxygen in the physiological range of oxygen concentrations is close to optimal. The relaxation rates in the absence of oxygen and for low concentrations of the agent are less than the oxygen contributions. The agent concentration-dependent broadening is reduced to one-third to one-tenth of the values observed for nitroxides. This will improve the accuracy of DNP and EPR oximetry by reducing the influence of the agent concentration on the saturation degree. Thus, the foundation is given and the practicality is demonstrated of oximetric imaging using agents such as these.

ACKNOWLEDGMENT

We thank Professor R. N. Muller for allowing measurements to be performed on the field-cycling relaxometer at the University of Mons-Hainaut, Belgium.

REFERENCES

1. G. Ehnholm, U.S. Patent 5,289,125 (1994).
2. I. Leunbach and J. H. Ardenkjær-Larsen, U.S. Patent Application Serial No. 08/546,146.
3. J. H. Ardenkjær-Larsen, ''Oximetric Implications of Dynamic Nuclear Polarisation,'' Thesis, Technical University of Denmark (1994).
4. D. Lurie, J. M. S. Hutchison, L. H. Bell, I. Nicholson, D. M. Bussell, and J. R. Mallard, Field-cycled proton–electron double-resonance imaging of free radicals in large aqueous samples, *J. Magn. Reson.* **84,** 431–437 (1989).
5. H. J. Halpern, D. P. Spencer, J. Polen, M. K. Bowman, A. C. Nelson, E. M. Dowey, and B. A. Teicher, Imaging radio frequency electron-spin-resonance spectrometer with high resolution and sensitivity for *in vivo* measurements, *Rev. Sci. Instrum.* **60,** 1040–1050 (1989).
6. H. M. Swartz and J. F. Glockner, *in* ''Advanced EPR. Applications in Biology and Biochemistry'' (A. Hoff, Ed.), Chapter 21, Elsevier, Amsterdam (1991).
7. A. I. Smirnov, R. B. Clarkson, and R. L. Belford, EPR linewidth (T2) method to measure oxygen permeability of phospholipid bilayers and its use to study the effect of low ethanol concentrations, *J. Magn. Reson. B* **111,** 149–157 (1996).
8. I. Leunbach, U.S. Patent 4,984,573 (1991).
9. D. Grucker and J. Chambron, Oxygen imaging in perfused hearts by dynamic nuclear polarization, *Magn. Reson. Imaging* **11,** 691–696 (1993).
10. P. Kuppusamy, M. Chzhan, K. Vij, M. Shteynbuk, D. J. Lefer, E. Giannella, and J. L. Zweier, Three-dimensional spectral–spatial EPR imaging of free radicals in the heart: A technique for imaging tissue metabolism and oxygenation, *Proc. Natl. Acad. Sci. USA* **91,** 3388–3392 (1993).
11. M. K. Stehling, F. Schmitt, and R. Ladebeck, Echo-planar MR imaging of human brain oxygenation changes, *J. Magn. Reson. Imaging* **3,** 471–474 (1993).
12. H. P. Shukla, R. P. Mason, D. E. Woessner, and P. P. Antich, A comparison of three commercial perfluorocarbon emulsions as high-field ^{19}FNMR probes of oxygen tension and temperature, *J. Magn. Reson. B* **106,** 131–141 (1995).
13. P. Röschmann, Radiofrequency penetration and absorption in the human body: Limitations to high-field whole-body nuclear magnetic resonance imaging, *Med. Phys.* **14,** 922–931 (1987).
14. H. Konijnenburg and A. F. Mehlkopf, Optimal field strength and pulse-sequence parameters for *in vivo* dynamic-polarization imaging, *J. Mag. Reson. B* **113,** 53–58 (1996).
15. A. Aabye, T. Almén, S. Anderson, K. Golman, M. Jørgensen, F. Rise, R. Servin, H. Wikström, and L.-G. Wistrand, EP 0515458 (1995).
16. S. Anderson, K. Golman, F. Rise, H. Wikström, and L.-G. Wistrand, U.S. Patent 5,530,140 (1996).
17. A. W. Overhauser, Polarization of nuclei in metals, *Phys. Rev.* **92,** 411–415 (1953).
18. A. Abragam, ''Principles of Nuclear Magnetism,'' Oxford University Press, Oxford (1961).
19. J. Trommel, ''Molecular Motions and Collisions in Organic Free Radical Solutions as Studied by Dynamic Nuclear Polarization,'' Thesis, Technische Hogeschool Delft, The Netherlands (1978).
20. J. Potenza, Measurement and applications of dynamic nuclear polarization, *Advan. Mol. Relaxation Processes* **4,** 229–354 (1972).
21. Y. Ayant, E. Belorizky, J. Alizon, and J. Gallice, Calcul des densités Spectrales résultant d'un mouvement aléatoire de translation en relaxation par interaction dipolaire magnetique dans les liquides, *Le Journal de Physique* **36,** 991–1004 (1975).
22. B. L. Bales, *in* ''Biological Magnetic Resonance. Spin Labeling. Theory and Applications'' (L. Berliner and J. Reuben, Eds.), Plenum, New York (1989).
23. K. Ramani, S. Ganapathy, and R. Srinivasan, A. Fourier transform approach to Voigt profile analysis and its application to nuclear magnetic resonance, *J. Magn. Res.* **24,** 231–237 (1976).
24. K. M. Salikhov, A. B. Doctorov, Yu. N. Molin, and K. I. Zamaraev, Exchange broadening of ESR lines for solutions of free radicals and transition metal complexes, *J. Magn. Res.* **5,** 189–205 (1971).
25. W. K. Subczynski and J. S. Hyde, The diffusion-concentration production of oxygen in lipid bilayers using the spin-label T_1 method, *Biochim. Biophys. Acta* **643,** 283–291 (1981).
26. L. P. Hwang and J. H. Freed, Dynamic effects of pair correlation function on spin relaxation by translational diffusion in liquids, *J. Chem. Phys.* **63,** 4017–4025 (1975).
27. M. B. Ravin and W. A. Briscoe, Blood-gas transfer, hemolysis, and diffusion capacity in a bubble tonometer, *J. Appl. Physiol.* **19,** 784–790 (1964).
28. S. H. Koenig and R. D. Brown, in ''NMR Spectroscopy of Cells and Organisms,'' Vol. II, CRC Press, Boca Raton, FL (1987).
29. R. G. Kooser, W. V. Volland, and J. H. Freed, ESR relaxation studies on orbitally degenerate free radicals. I. Benzene anion and tropenyl, *J. Chem. Phys.* **50,** 5243–5257 (1969).
30. M. Mehdizadeh, ''An Investigation on Electromagnetic Fields and Properties of the Loop-Gap Resonator, a Lumped Mode Microwave Resonant Structure,'' Thesis, Marquette University, Wisconsin (1983).
31. W. H. Press, S. A. Teukolsky, W. T. Vetterling, and B. P. Flannery, ''Numerical Recipes in C,'' 2nd ed., Cambridge University Press, Cambridge, U.K. (1992).

32. ''CRC Handbook of Chemistry and Physics,'' 70th ed., CRC Press, Boca Raton, FL (1989).

33. Y. Ayant, E. Belorizky, P. Fries, and J. Rosset, Effet des interactions dipolaires magnétiques intermoléculaires sur la relaxation nucléaire de molécules polyatomiques dans les liquides, *Le Journal de Physique* **38,** 325–337 (1977).

34. P. Vallet, ''Relaxivités des Radicaux Libres Stables de Type Nitroxide. Évaluation par la Méthode du Champ Cyclé et Optimisation,'' Thesis, Université de Mons-Hainaut (1992).

35. L. Verlet and J. J. Weiss, Exact solution of the Percus–Yevick integral equation for hard spheres, equilibrium theory of simple liquids, *J. Phys. Rev. A* **5,** 939–952 (1972).

36. M. S. Wertheim, *Phys. Rev. Lett.* **10,** E501 (1963).

37. E. Thiele, Equation of state for hard spheres, *J. Chem. Phys.* **39,** 474–479 (1963).

38. K. H. Hausser and D. Stehlik, Dynamic nuclear polarization in liquids, *in ''Advances in Magnetic Resonance,''* Vol. 3 (J. S. Waugh, Ed.), Academic Press, New York (1968).

39. S. I. Weissman and J. C. Sowden, Electron distribution in triphenylmetyl: Hyperfine structure of the paramagnetic resonance absorption of $(C_6H_5)_3C^{12*}$, *J. Am. Chem. Soc.* **75,** 503 (1953).

40. J. S. Hyde, ENDOR of free radicals in solution, *J. Chem. Phys.* **43,** 1806–1818 (1965).

41. J. H. Freed and G. K. Fraenkel, Theory of linewidths in electron spin resonance spectra, *J. Chem. Phys.* **39,** 326–348 (1963).

42. Yu. N. Molin, K. M. Salikhov, and K. I. Zamaraev, ''Spin Exchange,'' Springer-Verlag, Heidelberg (1980).

43. C. E. St.-Denis and C. J. D. Fell, Diffusivity of oxygen in water, *Can. J. Chem. Eng.* **49,** 885 (1971).

44. T. Goldstick and I. Fatt, Diffusion of oxygen in solutions of blood proteins, *Chem. Eng. Prog. Symp. Series* **66,** 101–113 (1970).